Robotics and Computer-Integrated Manufacturing 31 (2015) 101–110

Contents lists available at ScienceDirect

Robotics and Computer-Integrated Manufacturing

journal homepage: www.elsevier.com/locate/rcim

A multi-bead overlapping model for robotic wire and arc additive manufacturing (WAAM)

Donghong Ding, Zengxi Pan*, Dominic Cuiuri, Huijun Li

School of Mechanical, Materials & Mechatronic, Faculty of Engineering and Information Sciences, University of Wollongong, Northfield Avenue, Wollongong, NSW 2500, Australia

ARTICLE INFO

Article history:
Received 21 January 2014
Received in revised form
30 June 2014
Accepted 4 August 2014
Available online 15 September 2014

Keywords:
Overlapping model
Weld deposition
Additive manufacturing
Aerospace component

ABSTRACT

Wire and arc additive manufacturing (WAAM) is a promising alternative to traditional subtractive manufacturing for fabricating large aerospace components that feature high buy-to-fly ratio. Since the WAAM process builds up a part with complex geometry through the deposition of weld beads on a layer-by-layer basis, it is important to model the geometry of a single weld bead as well as the multi-bead overlapping process in order to achieve high surface quality and dimensional accuracy of the fabricated parts. This study firstly builds models for a single weld bead through various curve fitting methods. The experimental results show that both parabola and cosine functions accurately represent the bead profile. The overlapping principle is then detailed to model the geometry of multiple beads overlapping together. The tangent overlapping model (TOM) is established and the concept of the critical centre distance for stable multi-bead overlapping processes is presented. The proposed TOM is shown to provide a much better approximation to the experimental measurements when compared with the traditional flat-top overlapping model (FOM). This is critical in process planning to achieve better geometry accuracy and material efficiency in additive manufacturing.

© 2014 Elsevier Ltd. All rights reserved.

1. Introduction

Additive manufacturing (AM) builds up a component through the deposition of materials layer-by-layer instead of starting with an over dimensioned raw block and removing unwanted material, as practised in conventional subtractive manufacturing. AM is a promising alternative for fabricating components made of expensive materials such as titanium and nickel in the aerospace industry where such components often suffer an extremely high buy-to-fly ratio. Many techniques have been developed for manufacturing metal structures in AM, such as selective laser sintering [1], direct metal deposition [2], electron beam freeform fabrication [3], shape deposition manufacturing [4], and wire and arc additive manufacturing (WAAM) [5–7].

With regard to how the additive material is supplied, currently popular AM technologies can be classified as either a powder-feed process or a wire-feed process [8,9]. The powder-feed process is capable of fabricating parts with small size and high geometrical accuracy. In addition, it is possible to produce parts with functionally graded materials (FGM) [10]. On the other hand, the wire-feed approach is a cleaner and more environmental friendly process, which does not expose operators to the potentially hazardous powder environment. Compared with the powder-feed process, it has higher material usage efficiency with up to 100% of the wire material deposited into the component. Additionally, metal wires are lower in cost and more readily available than metal powders having suitable properties for AM, making wire-feed technology more cost-competitive.

Depending on the energy source used for metal deposition, wire-feed AM can be classified into three groups, namely laser based, arc welding based, and electron beam based [11]. Among these, arc welding based AM has shown promise due to its combined advantages of higher deposition rate, energy efficiency, safe operation and lower cost. Generally, the deposition rate of laser or electron beam deposition is in the order of 2–10 g/min, compared with 50–130 g/min for arc welding based AM technology [12–14]. Laser is commonly used as the energy source in the AM system. However, it has very poor energy efficiency (2–5%) [15]. Electron beam has a slightly higher energy efficiency (15–20%), but it requires a high vacuum working environment [16]. Compared with the poor energy efficiency of laser and electron beam, the energy efficiency of arc welding processes such as the gas metal arc welding (GMAW) or gas tungsten arc welding (GTAW) processes can be as high as 90% in some circumstances [17,18]. As a result, WAAM using either the GMAW or the GTAW process is a promising technology for manufacturing aerospace components with medium to large size in terms of productivity, cost-competitiveness and energy efficiency [5,6,19,20].

* Corresponding author.
E-mail addresses: dd443@uowmail.edu.au (D. Ding), zengxi@uow.edu.au (Z. Pan), dominic@uow.edu.au (D. Cuiuri), huijun@uow.edu.au (H. Li).

http://dx.doi.org/10.1016/j.rcim.2014.08.008
0736-5845/© 2014 Elsevier Ltd. All rights reserved.

Generally, the AM process involves slicing the 3D CAD model into a set of 2.5D layer contours with a constant or adaptive thickness, and depositing material into these contours to build the parts layer-by-layer from the bottom to the top. In WAAM, this building strategy incorporates the deposition of a large number of single weld beads side by side. Therefore, accurate models for single bead geometry as well as the multi-bead overlapping play an important role in determining the surface quality and dimensional accuracy of the fabricated products.

This study firstly builds models for a single bead profile through curve fitting methods. The experimental results show that both parabola and cosine functions accurately represent the bead profile. Based on the obtained single-bead model, a multi-bead overlapping model is developed and the critical centre distance to achieve stable multi-bead overlapping processes is analysed. The proposed model is proven to be a much better approximation to the experimental measurements compared to the traditional overlapping model from existing literatures.

The remainder of this paper is organized as follows. Section 2 models and compares the curve fitting results of three mathematical models for a single weld bead. Section 3 proposes a novel multi-bead overlapping model and develops the concept of critical centre distance. Section 4 presents the experimental results and discussions for the new multi-bead overlapping model followed by conclusions in Section 5.

2. Single bead modelling

Much research has been directed towards developing a correlation between welding parameters and weld bead geometry by using regression analysis [5], artificial neural networks, or combinations of these two techniques [21]. A symmetric parabola profile of the weld bead has been described by Suryakumar et al. [22]. Cao et al. [23] fitted the weld bead boundary with Gaussian, logistic, parabola and sine functions, and found that the sine function can fit the measured data with the highest accuracy. Xiong et al. [24] compared the measured weld beads under different welding parameters to three frequently-used profile models, namely circular arc, parabola, and cosine function. It was shown that the optimal model for the bead profile is largely dependent on the ratio of wire feed rate to welding speed. Previous research had used measured bead height and width instead of complete cross-sectional profile for the model parameters identification. Nevertheless, the relative errors of bead cross-sectional area predicted by their models were as high as 15–20% in certain circumstance [22,24]. Therefore, a further detailed measurement of the bead cross-sectional profile and the curve fitting based method are necessary for accurate modelling of bead geometry.

2.1. Single bead empirical models

Three popular mathematic functions, parabola, cosine and arc, are used here to model the cross-sectional profile of a single weld bead, as shown in Table 1. The bead height, h, bead width, w, and the bead area A for each model are summarized using various model parameters. In these functions, a, b, and c are model parameters which must be identified through experimental measurements.

2.2. Experimental set-up

Experimental tests were conducted using a robotic welding system at the University of Wollongong. The robotic WAAM

Table 1
Three bead models and the related bead height, bead width, and bead area.

Models	Model function	Bead height, h	Bead width, w	Bead area
Parabola model	$y=ax^2+c$	c	$2\sqrt{-\frac{c}{a}}$	$A_p=\frac{4c}{3}\sqrt{-\frac{c}{a}}$
Cosine model	$y=a\ \cos(bx)$	a	$\frac{\pi}{b}$	$A_c=\frac{2a}{b}$
Arc model	$y=\sqrt{a^2-x^2}+b$	$a-b$	$2\sqrt{a^2-b^2}$	$A_a=\text{arc}\cos(-b/a)-b\sqrt{a^2-b^2}$

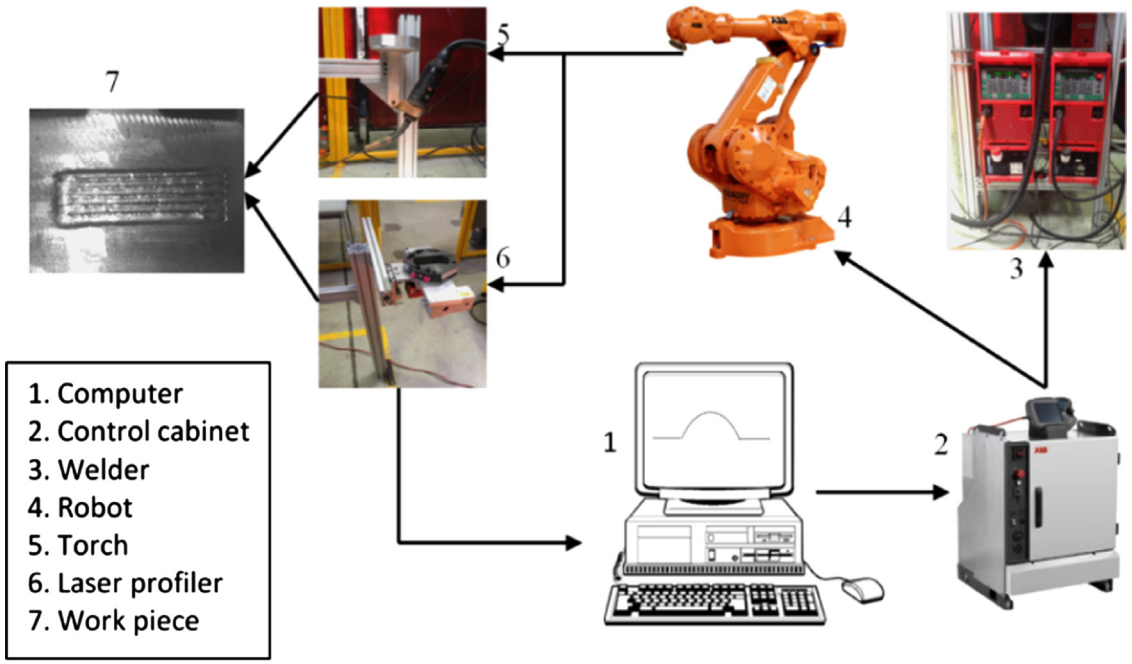

Fig. 1. Schematic diagram of the experimental WAAM system.

system and the 3D laser scanning system have been integrated into a welding cell to conduct the experiments, as described in Fig. 1. A computer interface (1) is used to programme the experimental processes and collect the experimental results. The robot controller (2) is used to coordinate both the robot motions and welding processes. (3) A programmable GMAW power source (3) is used to control the welding process. A large industrial robot (4) implements the movement of the welding torch (5) for metal deposition, and subsequently a laser profiler (6) to measure the bead profile. An example of weld bead deposits on a work piece is shown (7).

The pulsed-spray GMAW transfer mode was used to minimize the heat input. The wire electrode was copper coated steel wire with the diameter of 1.2 mm. The stick-out length was set to 18 mm to minimize weld spatter for this particular process. A shielding gas mixture of 82% argon and 18% CO_2 was used with a flow rate of 22 L/min. The wire feed rate was set at 5 m/min and the welding speed was varied from 200 to 550 mm/min. A 3D laser profile scanner with a resolution of 0.02 mm was used to accurately measure the cross-sectional profile of the weld beads at different locations along the welding direction. In order to improve the accuracy of measurements that are subject to random errors, each bead profile was scanned 200 times. The experimental data obtained from the laser profiler was processed using MATLAB. A 3D plot of some measured weld bead profiles is shown in Fig. 2. The left profile is a single bead with 200 cross-sections, while the centre and right are the profiles of welds having two overlapping beads.

2.3. Curve fitting results

Experiments were carried out for a combination of 1 wire-feed rate (V_f) and 8 different welding speeds (V_w). Each of the eight weld bead profiles is fitted using the three previously mentioned models with parameters that produce the highest value of R^2, which is the square of the correlation between the response values and the predicted response values. The parameters obtained from each model are summarized in Table 2. The ratio (λ) of wire-feed rate to welding speed is also calculated. With λ ranges from 9.1 to 25, the R^2 of all models are higher than 0.975, indicating that all of the models can accurately predict the weld bead geometry.

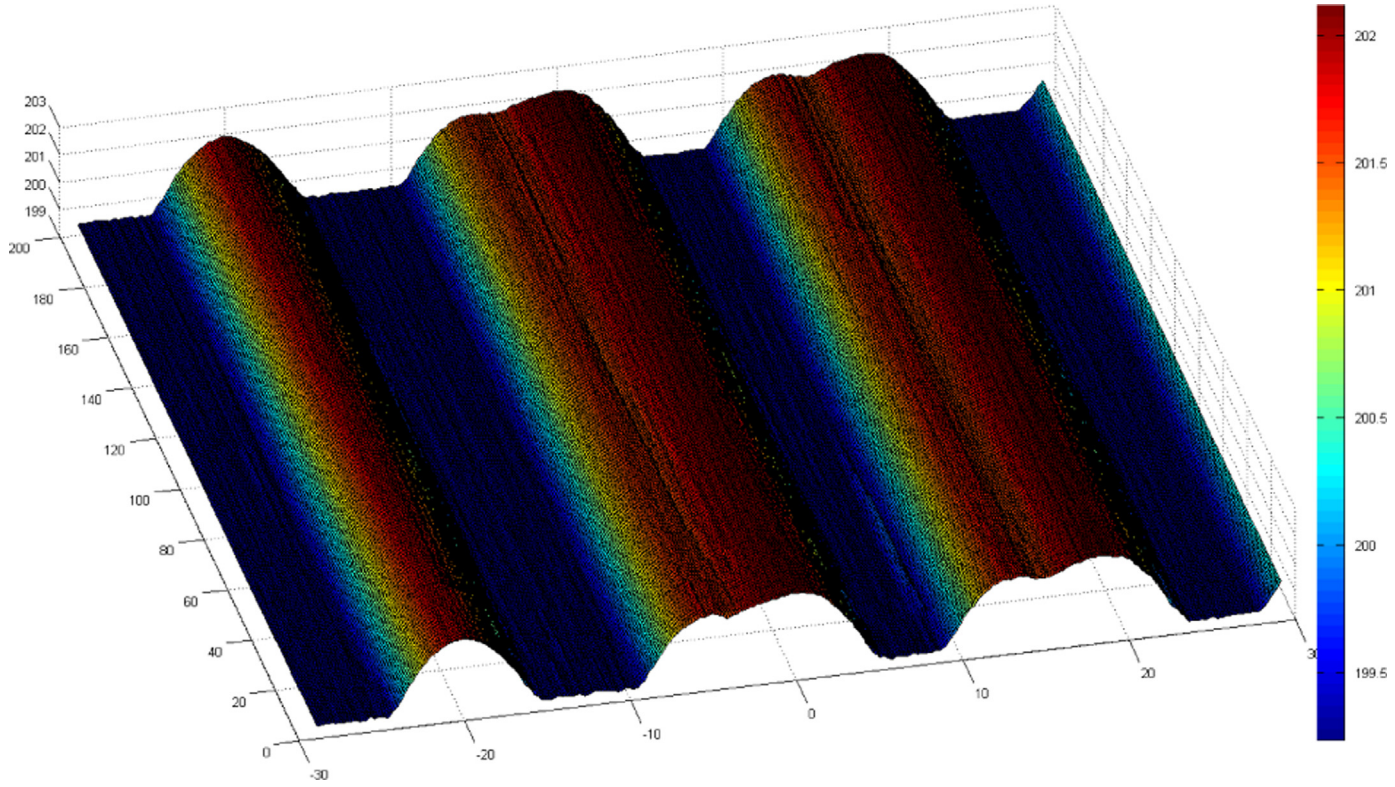

Fig. 2. Experimental measurements of weld bead profile.

Table 2
Curve fitting with three mathematic models.

S. no.	Process parameters		Parabola model			Cosine model			Arc model		
	V_w (mm/min)	Ratio λ	a	c	R^2	a	b	R^2	a	b	R^2
1	200	25	−0.0840	3.3418	0.9989	3.395	0.2411	0.9937	7.010	−3.720	0.9990
2	250	20	−0.0955	3.0176	0.9996	3.071	0.2716	0.9969	6.216	−3.251	0.9841
3	300	16.7	−0.1040	2.7210	0.9994	2.765	0.2971	0.9951	5.715	−3.042	0.9859
4	350	14.3	−0.1144	2.5420	0.9976	2.592	0.3248	0.9991	5.220	−2.727	0.9786
5	400	12.5	−0.1262	2.4615	0.9934	2.483	0.3461	0.9968	4.941	−2.571	0.9915
6	450	11.1	−0.1221	2.1919	0.9943	2.239	0.3625	0.9988	4.866	−2.717	0.9923
7	500	10	−0.1405	2.1513	0.9934	2.198	0.3925	0.9982	4.299	−2.194	0.9967
8	550	9.1	−0.1511	2.0704	0.9873	2.123	0.4173	0.9961	4.052	−2.034	0.9943

The relative error of area prediction, e_{Area}, is defined as the percentage of the area difference between the predicted and the actual bead area over the actual bead area,

$$e_{Area} = \frac{A_{predict} - A_{actual}}{A_{actual}} \times 100\%, \quad (1)$$

where, $A_{predict}$ is the prediction of the bead area by the mathematical models listed in Table 1. The actual area, A_{actual} of a weld bead cross-section, namely metal deposition rate per unit length, can be calculated as

$$A_{actual} = \frac{\pi V_f D_w^2}{4V_w} = \frac{\pi \lambda D_w^2}{4}, \quad (2)$$

where, V_f is the wire-feed rate, D_w is the diameter of the wire electrode, and V_w is the welding speed.

As shown in Fig. 3, the relative errors of all three models are within $\pm 4\%$. Compared with relative errors up to 15% in previous literature [22,24], the model parameters identified in this study are much more accurate without considering the material loss during the welding process. This is mainly due to the use of curve fitting with detailed bead cross-sectional measurements instead of only employing the bead height and width in the model fitting. As shown in Fig. 3, between the three empirical models, the parabola model and the cosine model provide a better approximation than the arc model. Good agreement between experimental results and the parabola model is obtained under all welding speeds, as shown in Fig. 4. In the following sections, the parabola model will be used for developing the overlapping model.

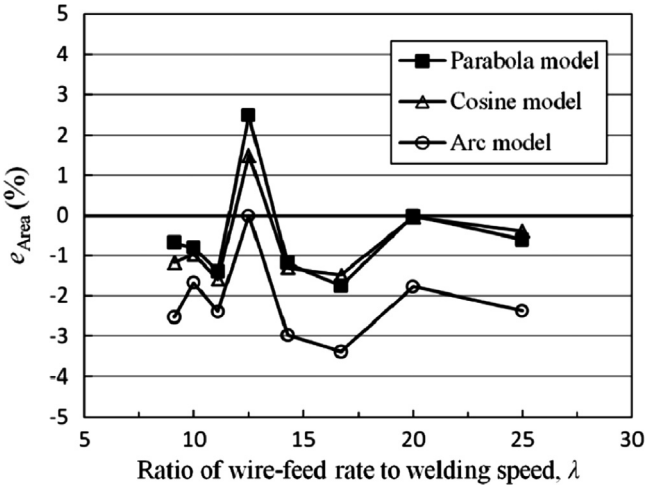

Fig. 3. Relative error for predicted and actual area of weld bead cross-section.

3. Multi-bead overlapping model

Some preliminary investigations on multi-bead overlapping models have been made in recent years [22–25]. A simple flat-top overlapping model (FOM) has been developed in the literature, and is described as follows. Let a single bead have a height h and width w; and the adjacent beads have a centre distance d. The area of valley and overlapping area in adjacent beads are depicted in Fig. 5. The centre distance d between adjacent beads plays an important role in determining surface quality and smoothness. When the centre distance d is greater than the single bead width w, there is no overlap within the two adjacent beads. As the centre distance is decreased, the overlapping area in Fig. 5 increases, and the area of the valley decreases. As the centre distance d decreases to a certain value, the overlapping area becomes equal to the area of the valley and the overlapped surface will become an optimal plane. With a further decrease of d, excessive overlapping area leads to an increased thickness of the deposited layer and decreasing surface smoothness. Consequently, the optimal centre distance d is determined by the criterion that a flat plane will be obtained when the overlapping area is equal to the area of valley. However, it has been observed through experimentation that it is impossible to achieve the ideally flat overlapped surface [22,25]. Therefore the overlap criterion proposed in these studies is not optimal and produces an undesired wavy surface. As a work piece requires deposition of several layers, uneven layer surface may lead to accumulating errors along the vertical

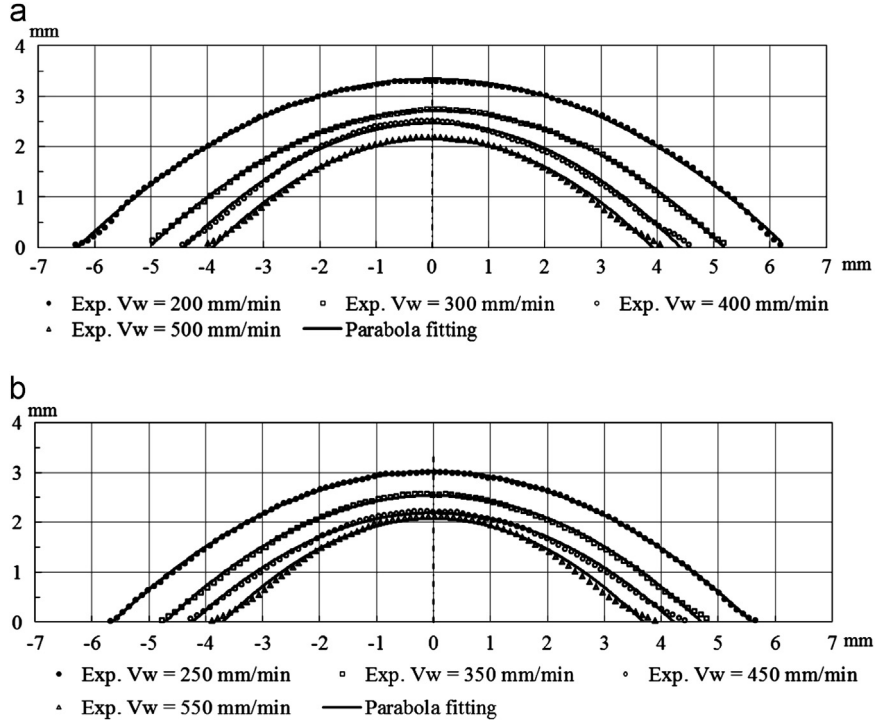

Fig. 4. Weld bead geometry of a single bead with various welding speeds.

direction, resulting in unstable deposition after several layers. Therefore, it is very important to build a more accurate bead overlapping model based on the determination of the optimal centre distance, so that a stable overlapping process can be achieved.

3.1. Principle of the tangent overlapping model (TOM)

In the traditional flat-top overlapping model (FOM) of Fig. 5, the area of valley consists of the boundaries of two beads and one straight line which connect the summits of both weld beads. However, during welding tests described in the previous section, it was observed that there is a "critical valley" geometry that better approximates the cross-section of multiple welding beads in gas metal arc welding (GMAW).

As shown in Fig. 6(a), for two weld beads with a width w and a height h, Bead 1 is first deposited on the substrate, and Bead 2 is deposited next to Bead 1 with a centre distance of d. A is the left-most point of Bead 2, at the toe of the weld. Point B is the point on Bead 1 which shares the same abscissa with point A. Line BC is tangential to Bead 2. In contrast to previous studies, this newly proposed model defines the critical valley as the zone BEC. The overlapping area is AED; the same as the previous FOM model. As the centre distance d is decreased from w to $w/2$, the size of the overlapping area (S_{AED}) increases from zero, while the size of the critical valley (S_{BEC}) increases initially from zero but then decreases. The detailed calculations of the area variations are provided in the following sections. As an introduction, the principle of TOM can be summarized as follows:

(1) When $S_{AED}=S_{BEC}$, the overlapped profile is described by Fig. 6(b). The corresponding centre distance is called the critical centre distance d^*.
(2) When the centre distance d varies from d^* to w, $S_{AED} < S_{BEC}$. In this case, the overlapped profile is shown in Fig. 6(c). Since the area of the critical valley BEC is larger than the overlapping area AED, the actual area of valley will be B′EC′ with the area of B′EC′ is equal to the area of AED, where B′ is a point on Bead 1, and line B′C′ is tangential to Bead 2.
(3) When the centre distance d varies from $w/2$ to d^*, $S_{AED} > S_{BEC}$, as shown in Fig. 6(d). The excessive overlapping area results in the altered profile of Bead 2. Through experimental tests, the parabolic curve of Bead 2 has been measured. As for previous geometric cases, B is also a point on bead one that shares the same abscissa with point A, but point A is defined on the non-altered profile of Bead 2 rather than the actual altered profile. Line BC is tangential to the altered profile of Bead 2. The profile of Bead 2 has been changed, indicating that the overlapping process is not stable for the first few beads. When multiple beads are deposited, the layer thickness will increase in comparison with the case $d^* \le d < w$. This results in the height of the first bead being much lower than the rest.

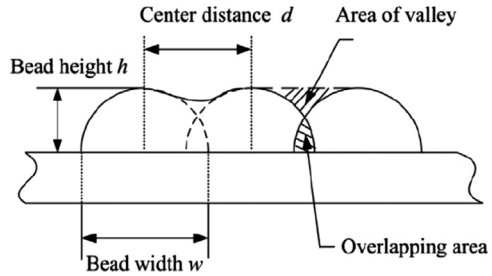

Fig. 5. Sketch of the traditional flat-top overlapping model (FOM) [24].

3.2. Overlapping of two beads

With the proposed overlapping principles of TOM, the key step of the overlapping model is to calculate the critical centre distance for any given weld bead.

Case (1) The centre distance $d=d^*$

In Fig. 6(a), two weld beads are considered as two parabolic

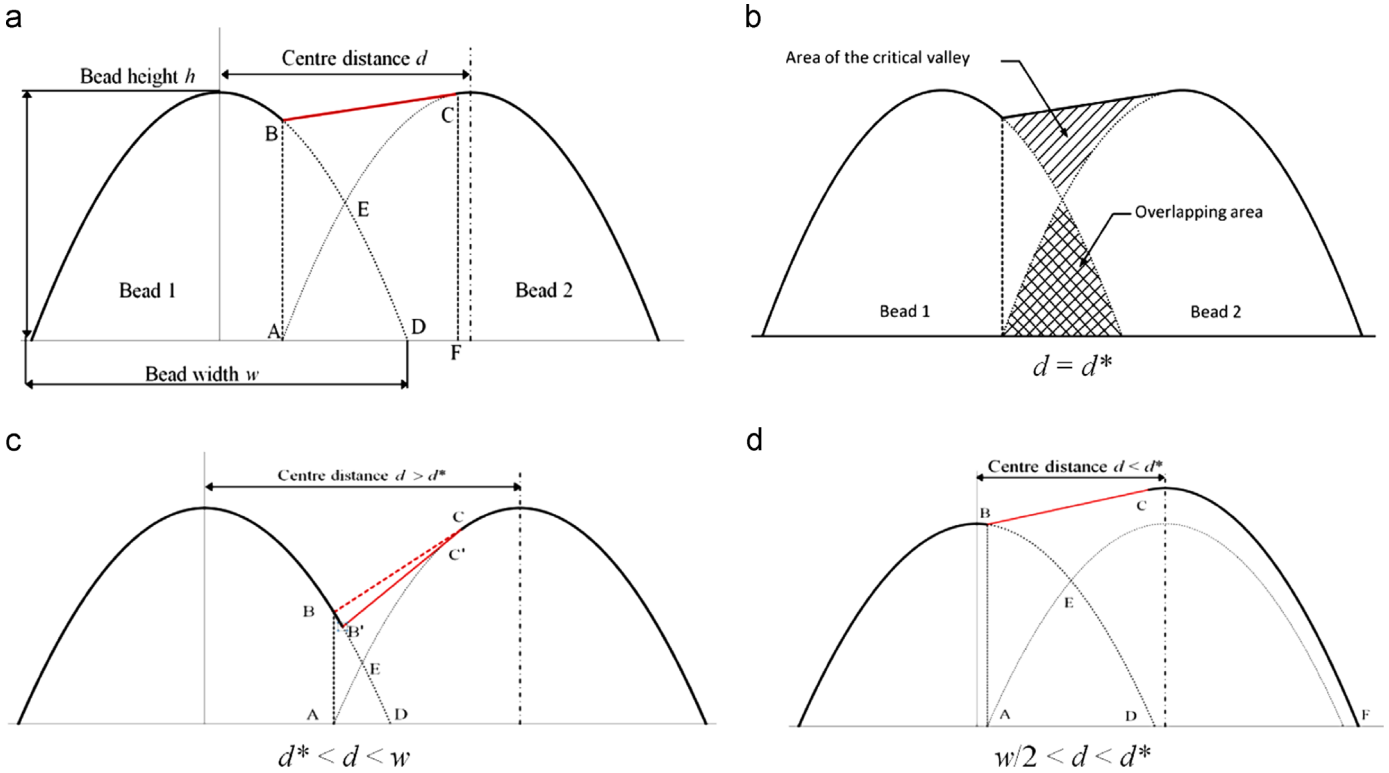

Fig. 6. Schematic diagrams of the tangent overlapping model (TOM).

functions expressed as

$$y = ax^2 + c, \tag{3}$$

$$y = a(x-d)^2 + c, \tag{4}$$

where c is equal to the weld height h and $a = -4h/w^2$. For a given weld bead, a and c are derived from the model of a single bead. If the coordinates of points A, B, F, C are defined as A(x_1,0), B(x_1,y_1), F(x_2,0), C(x_2,y_2), the gradient of the line BC is k, then S_{AED} and S_{BEC} can be represented using the following functions:

$$S_{AED} = 2\int_{x_1}^{d/2} (ax^2 + c)dx, \tag{5}$$

$$\begin{aligned} S_{BEC} &= S_{ABCF} + S_{AED} - S_{ABD} - S_{ACF} \\ &= \frac{y_1 + y_2}{2}(x_2 - x_1) + 2\int_{x_1}^{d/2} (ax^2 + c)dx - \int_{x_1}^{\sqrt{-c/a}} (ax^2 + c)dx \\ &\quad - \int_{x_1}^{x_2} \left[a(x-d)^2 + c\right]dx, \end{aligned} \tag{6}$$

We define $f(d)$ as the function of the difference between S_{AED} and S_{BEC}:

$$f(d) = S_{BEC} - S_{AED} = \frac{1}{3}ad^3 + \frac{1}{6}aw^3 - \frac{1}{2}awd^2 - \frac{ad(w-d)}{3}\sqrt{wd - d^2}, \tag{7}$$

When $S_{AED}=S_{BEC}$, $f(d)=0$. Among the four roots obtained from this equation, only two of them have positive real values:

$$d_1 = w$$

$$d_2 = w\left[\left(\sqrt{\frac{1}{512}} + \frac{1}{16}\right)^{1/3} + \frac{1}{8}\left(\sqrt{\frac{1}{512}} + \frac{1}{16}\right)^{-1/3}\right] \approx 0.738w$$

This indicates that within the range of ($w/2$, w), there exists a unique critical distance, $d^*=0.738w$. Fig. 7 plots the trends of S_{AED}, S_{BEC}, and $f(d)$ as the centre distance d varies from $w/2$ to w. With increasing centre distance, the S_{AED} decreases, while S_{BEC} increases at the beginning but decreases to zero in the end. S_{AED} is equal to S_{BEC} when the centre distance d is equal to the critical centre distance $0.738w$.

Case (2) The centre distance d in the range $d^* < d < w$
As described in Fig. 6(c), B′ is a point on Bead 1, C′ is a point on Bead 2. Line B′C′ is tangential to Bead 2. By applying the relationship that S_{AED} is equal to $S_{B'EC'}$, the coordinates of point B′ and C′ can be solved, and the overlapped profile can be obtained similarly to case (1).

Case (3) The centre distance $w/2 < d < d^*$
When the centre distance d is less than the critical centre distance, the second bead profile is changed. In this case, the overlapping process is more complicated. Through experimental measurements, it was found that the boundary of the second weld bead can also be represented by a parabola function with the same parameter a as the parabolic curve of the first weld bead. Therefore, the second bead can be represented as

$$y = a(x-d)^2 + c_2, \tag{8}$$

where, the parameter c_2, the height of the second weld bead, can be solved at the certain centre distance d. For simplicity, the detailed calculations are omitted here.

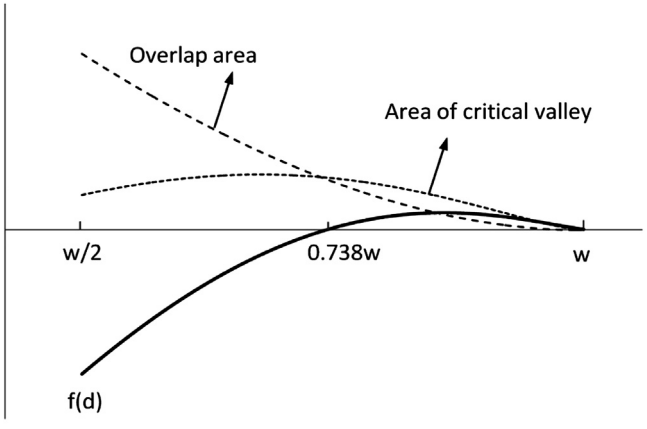

Fig. 7. The overlap area, the area of the critical valley, and $f(d)$ as a function of the centre distance d.

3.3. Multi-bead overlapping

In WAAM, each layer is fabricated by depositing a large number of single weld beads side by side. The overlapping processes of weld beads determine the surface quality and dimensional accuracy of the fabricated products. Therefore, it is important to investigate the overlapping process of multi-bead deposits. In the case of $d \geq d^*$, the all weld beads have the same height, so the parabolic function of all weld beads has the same value of parameter c ($c_1=c_2=\ldots=c_n$). This means that the overlapping process of the third weld bead on the second weld bead is the same as that the process of overlapping the second weld bead on the first weld bead. Therefore, the process of multi-bead overlapping can be considered as the repeated two-bead overlapping processes. However, in the case of $d < d^*$, the parabolic function of the second weld bead boundary will be changed during the overlapping process. For any given weld bead in the multi-bead deposit, the overlapped profile can be simulated numerically. The schematic overlapped profile of a multi-bead deposit at $d < d^*$ is represented in Fig. 8. It can be found that such overlapping processes are not stable, with the thickness of the layer increasing as more beads are deposited.

4. Experimental verification for the overlapping model

Based on the traditional FOM, to achieve a flat deposition surface the optimal centre distance is $d=0.667w$ using the parabola model for single bead. According to the proposed TOM, a centre distance of $0.667w$ would induce an unstable overlapping process as it is less than the critical centre distance $d^*=0.738w$. Fig. 9 compares the experimental measurements of overlapping bead profile with the predictions from the proposed TOM and the traditional FOM. The welding speed was set at 400 mm/min for this test. The single bead model parameters can be obtained from row 5 in Table 2. The bead width is calculated using the formula in Table 1.

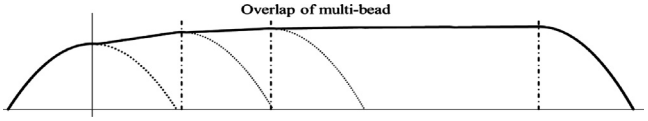

Fig. 8. The schematic overlapped profile of a multi-bead deposit at $d < d^*$.

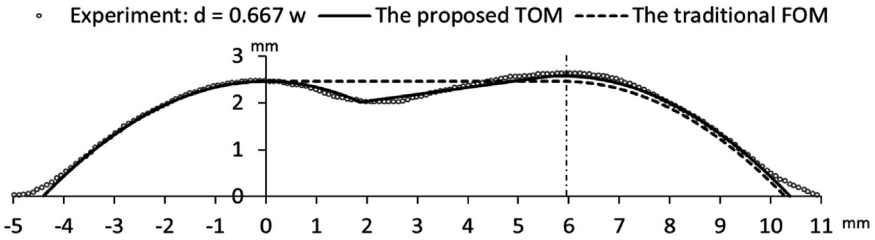

Fig. 9. Comparison of experimental measurements of bead profile with the tangent overlapping model (TOM) and the flat-top overlapping model (FOM).

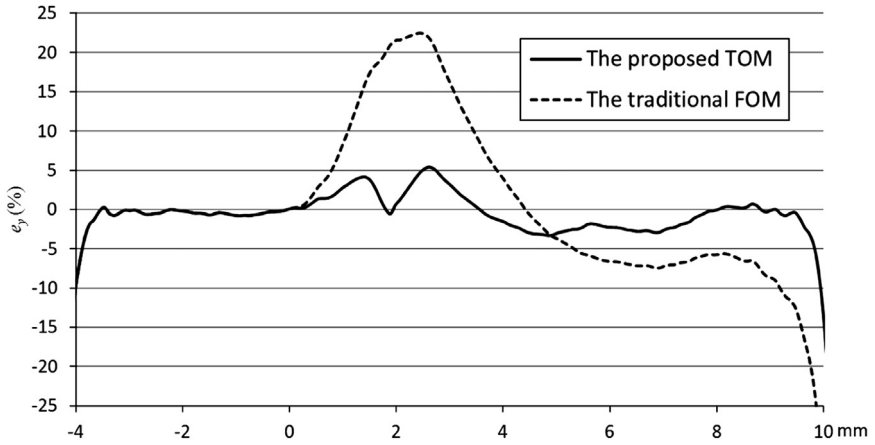

Fig. 10. The relative errors between the experimental bead profile and the models.

Prediction of the overlapped profile at $d=0.667w$ through the traditional FOM yields

$$y=\begin{cases} ax^2+c & -w/2<x<0, \\ c & 0<x<d, \\ a(x-d)^2+c & d<x<d+w/2. \end{cases} \tag{9}$$

Prediction of the overlapped profile at $d=0.667w$ through the proposed TOM yields

$$y=\begin{cases} ax^2+c_1 & -w/2<x<x_1, \\ k(x-x_1)+y_1 & x_1<x<x_2, \\ a(x-d)^2+c_2 & x_2<x<d+w_2/2. \end{cases} \tag{10}$$

where, $C_1=C$ is the height of the first bead; c_2 is the height of the second bead, which could be solved numerically; x_1, x_2 and k are parameters as mentioned in Section 3.2, all of these can be solved for any given weld bead; w_2 is the width of the second bead which could be solved when c_2 is obtained.

In Fig. 9, the experimental data, FOM and proposed TOM are represented by the dotted line, dashed line and solid line respectively. It can be seen that the proposed TOM approximates the experimental results much better than the traditional FOM, particularly in the zone of the valley.

Using the traditional FOM, a flat plane would be obtained at the optimal centre distance, which does not match with the experimental data. The proposed TOM model is more suitable in describing the zone of the valley. Additionally, the proposed model predicts a higher peak for the second bead as the centre distance is less than d^*, which has been confirmed in the experimental measurements.

To compare the accuracy of both models quantitatively, relative errors between the measured profile and the predicted profile along the bead width direction are plotted in Fig. 10, with e_y defined as,

$$e_y(\%)=\frac{y_{\mathrm{mod\ }el}-y_{measurement}}{y_{measurement}}\times 100\%, \tag{11}$$

It can be found that FOM results in a high relative error in the zone of the valley (0–6 mm in Fig. 10). This is because the valley is assumed to be a flat plane in the literature, but it is waved in the experiments. The proposed TOM is more accurate than the traditional FOM. Although both models are not accurate at the zone near the substrate, it is inconsequential and may be disregarded when compared to the zone of the valley, because the volume of deposited material is much lower near the weld toe in comparison to the valley.

Further experimental measurements of overlapped bead profile for various centre distances d are provided. Fig. 11 presents the model predictions and measurement data in all three circumstances, namely (a) $d=d^*$, (b) $d>d^*$, (c) $d<d^*$. It can be seen that, the proposed TOM agree with experiments very well in all three situations.

Unlike the traditional FOM, the proposed TOM model predicts an asymmetrical overlapping geometry between the peaks of the two beads. In addition, the experimental measurements show that the height of the second bead is higher than the first one when the centre distance is smaller than the critical centre distance, which agrees with the proposed model. The ratio of the height for the second bead over the first bead at various centre distances are calculated and compared to experimental measurements, as shown in Fig. 12. It can be seen that when the centre distance d is larger than the critical centre distance d^*, the ratio is approximately 1.0, i.e. the second bead has the same height as the first one. When the centre distance is less than the critical centre distance, the ratio increases, indicating an increase in the height of the second bead. The proposed TOM model has been quantitatively verified through these experimental measurements. According to the centre distance, there are stable and unstable overlap

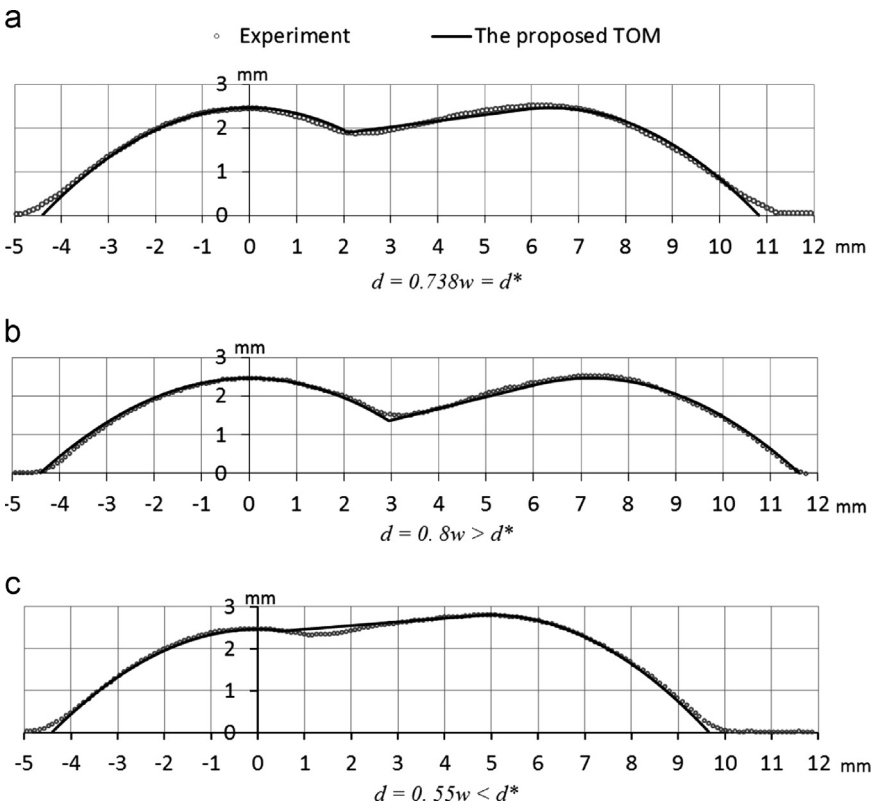

Fig. 11. The experimental results of overlapped bead profile at various centre distance *d*.

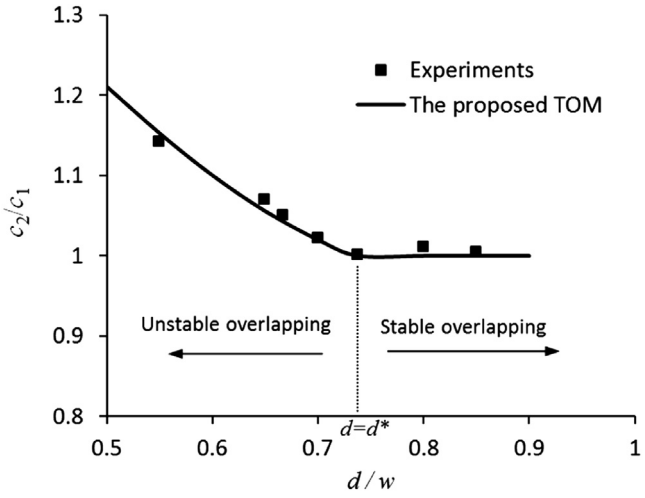

Fig. 12. The ratio of the height of the second bead to the first bead (c_2/c_1) at various centre distance d/w.

zones, which have significant implications for process planning in WAAM.

The best use of the bead overlapping model is to provide an estimate of optimal centre distance for AM. The traditional model proposes $d_{opt}=0.667w$ while the proposed model claims $d_{opt}=0.738w$. Further experiments were conducted at both of these centre distances for multi-bead and multi-layer deposition to compare the performance of the models. As shown in Fig. 13, AM deposits were made at these centre distances with five layers of deposition and six beads in each layer. The welding speed was 500 mm/min for these tests. The cross section was scanned after the first, third and fifth layers were deposited. It should be noted that, during the deposition processes, a few minutes of waiting time was used between each pass as well as subsequent layers to eliminate the temperature's effects on weld bead geometries as much as possible.

In Fig. 13(a), a centre distance of $d=0.667w$ was used. After deposition of five layers, it can be seen that the layer thickness at the first bead becomes much lower than the rests. This result is predicted by the proposed TOM. Since the centre distance is less than d^*, the height of the following bead will be higher than the previous one. In Fig. 13(b), the critical centre distance ($d=0.738w$) proposed by the TOM is used. After deposition of five layers, the variations in the height of the bead peaks from left to right hand are relatively smaller. As more layers are deposited, the variation in bead peak height becomes progressively worse when the centre distance $d=0.667w$, while it is significantly more stable when the centre distance $d=0.738w$. These results demonstrate that the critical centre distance proposed by the TOM results in a stable overlapping process, which is a necessary condition for the additive manufacture of large components.

Generally, any component that is built by depositing a series of overlapping beads is subjected to a machining process to remove the scallops. Yield η is the ratio of the volume of the part remaining after machining to the volume of the total metal deposited. Yield reflects the material utilization for a process, very similar to casting. In Fig. 13(a) and (b), the maximum yield at two centre distance are 75.7% and 84.1% respectively, indicating that the proposed TOM is more material efficient than the traditional FOM.

5. Conclusions

In this research, the model of a single weld bead cross-sectional profile has been developed using parabola, cosine, and arc

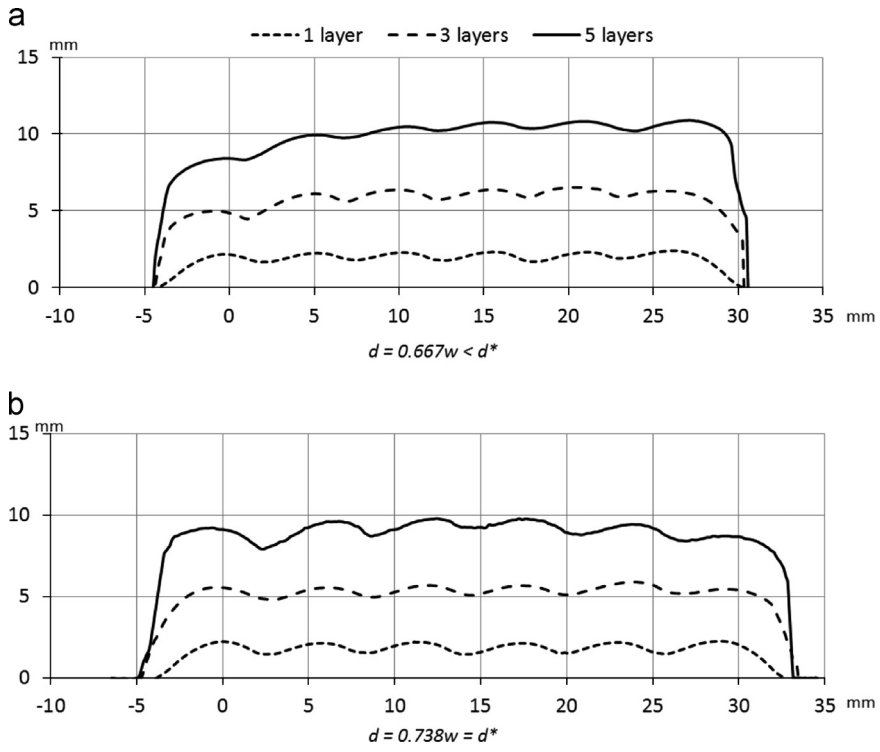

Fig. 13. Experiments of multi-bead and multi-layer deposition.

functions. Using high resolution measurements from a 3D laser scanning system, the model parameters have been accurately determined by curve fitting the experimental measurements to the various functions. It was found that both parabola and cosine models can most accurately represent a single weld bead.

Based on experimental observations, the profiles produced by multi-bead overlapping processes have been analysed, and a multi-bead tangent overlapping model (TOM) was proposed. Distinct from the traditional flat-top overlapping model (FOM), the concept of the critical valley has been defined and incorporated into the proposed model. The critical centre distance d^* that is necessary for a stable overlapping process is predicted from this model. The proposed model was validated experimentally by producing multi-bead deposits at various centre distances. It was found that the traditional model tends to under-estimate the critical centre distance, thereby producing unstable deposits of unacceptably variable height. In contrast, the new model was able to accurately predict the critical centre distance, so that stable deposits were made. This detailed investigation of the multi-bead overlapping process will provide important information for process planning in WAAM.

Acknowledgements

This work was supported by the Defence Materials Technology Centre (DMTC), which was established and is supported by the Australian Government's Defence Future Capability Technology Centre (DFCTC) initiative. The authors would like to thank Professor J. Norrish for his expertise in the welding field. N. Larkin is especially thanked for his assistance with the experiments. This work is supported in part by the State Scholarship Fund of the China Scholarship Council (No. 2011684067).

Appendix A. Supporting information

Supporting information associated with this article can be found in the online version at http://dx.doi.org/10.1016/j.rcim.2014.08.008.

References

[1] Agarwala M, Bourell D, Beaman J, Marcus H, Barlow J. Direct selective laser sintering of metals. Rapid Prototyp J 1995;1:26–36.
[2] Lewis GK, Schlienger E. Practical considerations and capabilities for laser assisted direct metal deposition. Mater Des 2000;21:417–23.
[3] Taminger KM, Hafley RA. Electron beam freeform fabrication: a rapid metal deposition process. In: Proceedings of the 3rd annual automotive composites conference; 2003. p. 9–10.
[4] Merz R, Prinz FB, Ramaswami K, Terk M, Weiss L. Shape deposition manufacturing: engineering design research center. Stanford, California, USA: Carnegie Mellon University; 1994.
[5] Almeida PS, Williams S. Innovative process model of Ti–6Al–4V additive layer manufacturing using cold metal transfer (CMT). In: Proceedings of the twenty-first annual international solid freeform fabrication symposium. Austin, TX, USA: University of Texas; 2010.
[6] Ding J, Colegrove P, Mehnen J, Ganguly S, Sequeira PM, Wang F, et al. Thermo-mechanical analysis of wire and arc additive layer manufacturing process on large multi-layer parts. Comput Mater Sci 2011;50:3315–22.
[7] Wang F, Williams S, Rush M. Morphology investigation on direct current pulsed gas tungsten arc welded additive layer manufactured Ti6Al4V alloy. Int J Adv Manuf Technol 2011;57:597–603.
[8] Mok SH, Bi G, Folkes J, Pashby I. Deposition of Ti–6Al–4V using a high power diode laser and wire, Part I: investigation on the process characteristics. Surf Coat Technol 2008;202:3933–9.
[9] Brandl E, Michailov V, Viehweger B, Leyens C. Deposition of Ti–6Al–4V using laser and wire, part I: microstructural properties of single beads. Surf Coat Technol 2011;206:1120–9.
[10] Zhang Y, Wei Z, Shi L, Xi M. Characterization of laser powder deposited Ti–TiC composites and functional gradient materials. J Mater Process Technol 2008;206:438–44.
[11] Karunakaran KP, Suryakumar S, Pushpa V, Akula S. Low cost integration of additive and subtractive processes for hybrid layered manufacturing. Robot Comput-Integr Manuf 2010;26:490–9.

[12] Mazumder J, Dutta D, Kikuchi N, Ghosh A. Closed loop direct metal deposition: art to part. Opt Lasers Eng 2000;34:397–414.
[13] Wanjara P, Brochu M, Jahazi M. Electron beam freeforming of stainless steel using solid wire feed. Mater Des 2007;28:2278–86.
[14] Sreenathbabu A, Karunakaran KP, Amarnath C. Statistical process design for hybrid adaptive layer manufacturing. Rapid Prototyp J 2005;11:235–48.
[15] Unocic R, DuPont J. Process efficiency measurements in the laser engineered net shaping process. Metall Mater Trans B 2004;35:143–52.
[16] Rannar LE, Glad A, Gustafson CG. Efficient cooling with tool inserts manufactured by electron beam melting. Rapid Prototyp J 2007;13:128–35.
[17] DuPont J, Marder A. Thermal efficiency of arc welding processes. Weld J (Including Welding Research Supplement) 1995;74:406s.
[18] Stenbacka N, et al.. Review of arc efficiency values for gas tungsten arc welding; 2012.
[19] Xiong J, Zhang G, Qiu Z, Li Y. Vision-sensing and bead width control of a single-bead multi-layer part: material and energy savings in GMAW-based rapid manufacturing. J Clean Prod 2012;41:82–8.
[20] Colegrove PA, Coules HE, Fairman J, Martina F, Kashoob T, Mamash H, et al. Microstructure and residual stress improvement in wire and arc additively manufactured parts through high-pressure rolling. J Mater Process Technol 2013;213:1782–91.
[21] Xiong J, Zhang G, Hu J, Wu L. Bead geometry prediction for robotic GMAW-based rapid manufacturing through a neural network and a second-order regression analysis. J Intell Manuf 2012;25:1–7.
[22] Suryakumar S, Karunakaran KP, Bernard A, Chandrasekhar U, Raghavender N, Sharma D. Weld bead modeling and process optimization in hybrid layered manufacturing. Comput-Aided Des 2011;43:331–44.
[23] Cao Y, Zhu S, Liang X, Wang W. Overlapping model of beads and curve fitting of bead section for rapid manufacturing by robotic MAG welding process. Robot Comput-Integr Manuf 2011;27:641–5.
[24] Xiong J, Zhang G, Gao H, Wu L. Modeling of bead section profile and overlapping beads with experimental validation for robotic GMAW-based rapid manufacturing. Robot Comput-Integr Manuf 2012;29:417–23.
[25] Aiyiti W, Zhao W, Lu B, Tang Y. Investigation of the overlapping parameters of MPAW-based rapid prototyping. Rapid Prototyp J 2006;12:165–72.